Annales Geophysicae, 23, 2357–2368, 2005
SRef-ID: 1432-0576/ag/2005-23-2357

Annales Geophysicae

Radio tomographic imaging of sporadic-E layers during SEEK-2

P. A. Bernhardt[1], C. A. Selcher[2], C. Siefring[1], M. Wilkens[3], C. Compton[4], G. Bust[5], M. Yamamoto[6], S. Fukao[6], O. Takayuki[7], M. Wakabayashi[7], and H. Mori[8]

[1]Plasma Physics Division, Naval Research Laboratory, Washington, DC 20375, USA
[2]Information Technology Division, Naval Research Laboratory, Washington, DC 20375, USA
[3]Icarus Research, Inc., Bethesda, MD, USA
[4]West Virginia University, Morgantown, WV, USA
[5]Applied Research Laboratory, University of Texas Austin, Austin, TX, USA
[6]Radio Science Center for Space and Atmosphere, Kyoto University, Kyoto, Japan
[7]Graduate School of Science, Tohoku University, Japan
[8]Communications Research Laboratory, Tokyo, Japan

Received: 26 October 2004 – Revised: 13 June 2005 – Accepted: 27 June 2005 – Published: 13 October 2005

Part of Special Issue "SEEK-2 (Sporadic-E Experiment over Kyushu 2)"

Abstract. During the SEEK-2 Rocket Campaign in August 2002, a Dual Band Beacon (DBB) transmitting to Ground Receivers provided unique data on E-Region electron densities. Information from two rocket beacons and four ground receivers yielded multiple samples of E-region horizontal and vertical variations. The radio beacon measurements were made at four sites (Uchinoura, Tarumizu, Tanegashima, Takazaki) in Japan for two rockets (S310-31 and S310-32) launched by the Institute of Space and Aeronautical Science (ISAS). Analysis was completed for four sets of beacon data to provide electron density images of sporadic-E layers. Signals from the two-frequency beacons on the SEEK-2 rockets were processed to yield total electron content (TEC) data that was converted into electron density measurements. Wide variations in layer structures were detected. These included horizontal sporadic-E variations, vertical profiles of double, single, and weak layers. The radio beacon measurements were shown to be in agreement with the in-situ SEEK-2 sensors. The first tomographic image of a sporadic-E layer was produced from the data. The rocket beacon technique was shown to be an excellent tool to study sporadic-E layers because absolute TEC accuracy of 0.01 TEC Units can be easily obtained and, with proper receiver placement, electron density images can be produced using computerized ionospheric tomography with better than 1 km horizontal and vertical resolution.

Keywords. Ionospheric irregularities – Instruments and techniques – Mid-latitude ionosphere

Correspondence to: P. Bernhardt
(bern@ppdmail.nrl.navy.mil)

1 Introduction

Sporadic-E layers, found between 100 and 120 km altitude, have been studied around the world for over six decades. During this period, the spatial and temporal variations in electron density were measured using ionosondes, radars, and radio beacons on rockets (Smith and Matsushita, 1962). Recent interest in sporadic-E structures has been rekindled by radar observations of quasi-period radar echoes (Yamamoto et al., 1991; Yamamoto et al., 1994; Yamamoto et al., 1998; Haldoupis et al., 2003) and the radio-induced aurora (RIA) imaging of the horizontal structure of sporadic-E layers (Djuth et al., 1988; Kagan et al., 2000 and Bernhardt et al., 2003). The turbulence associated with sporadic-E layers provides an exciting basis for new observational and theoretical studies.

The formation of sporadic-E layers has long been associated with neutral wind shears (Whitehead, 1970). Theories on E layer patches have involved Kelvin-Helmoltz (KH) turbulence, plasma instabilities, and gravity waves. The generation of turbulence in sporadic-E layers by exceptionally high wind shears, on the order of 100 m/s, was first proposed by Layzer (1962). When the wind shear is sufficiently great, Layzer (1962) points out that a critical value of the Richardson number Ri is exceeded and a turbulent layer is formed that spreads the spectrum of radio reflections. The Richardson number is given by $Ri = \left(\omega_g / \omega_S\right)^2$ where ω_g , the Brunt-Vaisalla frequency, is the oscillating frequency for a fluid element displaced from equilibrium and ω_S is the mean-velocity gradient or wind shear. Meteorological studies have shown that the critical value of Ri for turbulence onset is between 0.04 and 1. Larsen (2000) suggests that neutral

wind shears can seed the Kelvin-Helmholtz instability when the Richardson number is less than unity. The neutral Kelvin-Helmholtz billows transport the ions in the E layer to form quasi-periodic structures in the densities. Such quasi periodic structures have been previously reported using ground radar backscatter by Yamamoto et al. (1991) and subsequent publications. Numerical modeling of the Kelvin-Helmholtz (KH) instability coupled to the E layer plasma was carried out by Bernhardt (2002). The simulations showed that depending on the altitude of the node in the shear, the E layer could divide into multiple layers (near 100 km altitude) or form quasi-periodic clumps (near 120 km altitude) as the neutral KH billows formed. The plasma structures formed with the low Richardson number flow are attractive because of their similarity to the billow-like data obtained using radar scans of sporadic-E layers at Arecibo by Miller and Smith (1978).

An alternative theory for the formation of sporadic-E structures involves plasma instabilities for the thin layer (Cosgrove and Tsunoda, 2004). The Cosgrove-Tsunoda (CT) instability features maximum growth of a wind shear oriented at an angle of 45 deg from the magnetic meridian. At this angle, any perturbation in the thin plasma layer gets amplified to form multiple E layer density structures. The primary difference between the KH and CT mechanisms is the orientation of the irregularities. The KH instability can yield irregularities at any orientation with the magnetic meridian while the CT instability tends to have them oriented obliquely. Finally, Woodman Yamamoto and Fukao (1991) propose that atmospheric gravity waves can modulate the shape of the sporadic-E layers. The orientation of the E-layer irregularities would be determined by the propagation direction of the gravity wave. This process is similar to the structuring by the KH instabilities except that the source of the fluctuations in the neutral atmosphere is not tied to the wind shear. Ground backscatter radar scatter from field aligned irregularities provides data consistent with all these processes. The radar, however, does not directly measure the kilometer-scale structures in electron density that feeds the smaller scale the field-aligned-irregularities responsible for radar scatter. A radio beacon from a rocket may be able to use tomography or triangulation to determine electron densities and orientation of the Sporadic-E structures.

To help isolate the electron density structures associated with sporadic-E layers, an ionospheric imaging experiment was devised using radio beacon transmissions during the SEEK-2 Campaign in Japan. The Institute of Space and Aeronautical Science (ISAS) sponsored the second sporadic-E Experiment over Kyushu (SEEK-2) to enhance our understanding of the formation and evolution of sporadic-E layers. The two rocket campaign studied sporadic-E layer structures using space-based and ground-based instruments. The two rockets were identified as S310-31 and S310-32. The following instruments were launched during SEEK-2: EFD (Electric Field), FBP (Fixed Bias Probe), FLP (Langmuir Probe), DBB (Dual Band Beacon), NEI and PWM (Plasma Density and Waves), IAF (Attitude), MGF (Magnetic Field) and TMA (Tri-Methyl Aluminum). The results from each of these instruments are described in this issue. This paper focuses on the dual band beacon (DBB) observations with comparisons to other in-situ electron density sensors.

The DBB instrument radiated two unmodulated frequencies for measurements of total electron content (TEC) from the rocket beacons to each receiver on the ground. The dual frequency technique for ionospheric studies is not new. Continuous wave (CW) radio transmissions from rockets have been used for over 60 years old to study sporadic-E layers (Seddon, 1953). In the early experiments, HF frequencies (4.27 MHz or 7.75 MHz and their 6th harmonic) were radiated to ground receivers. The lowest received frequency was multiplied a factor of six and mixed with the upper frequency. The variations in the mixing product were differentiated in time to yield the electron density along the line-of-sight trajectory. A summary of the sporadic-E data obtained with this technique is given by Seddon (1962). The altitude resolution from these measurements is typically 0.2 to 1.0 km. Some problems associated with these low frequencies are (1) refraction of the paths in the ion layers, (2) blockage of the signals where the E layer critical frequency exceeded the transmitter frequency, and (3) inefficient radiation from the rocket antennas which were much smaller than the radio wavelength. Further details on ionospheric layer profiling using rocket beacon signals are described by Jackson (1954), Friedman (1959), Maeda (1970), Evans (1977), Smith and Gilchrist (1974), and Bernhardt et al. (1993). The use of radio beacons to study ionospheric modification with chemical releases is described by Fulford et al. (1987) and Bernhardt et al. (1993). In these papers, electron density profiles were derived when the rocket passed through the plasma layers. The ionospheric fluctuation data were not processed to yield electron densities when the rocket flew over the ionospheric layers. Theoretical studies by Bernhardt et al. (1993) and Bernhardt and Huba (1993) have used numerical simulations to demonstrate that tomographic analysis of rocket beacon TEC data can be used for reconstructive imaging of F-region irregularities.

The SEEK-2 DBB experiments were unique because, for the first time, computerized ionospheric tomography was employed to produce high resolution images of the electron density in sporadic-E layers. Other improvements over previous measurements with radio beacons arise from Eq. (1) choosing VHF (150 MHz) and UHF (400 MHz) frequencies that are unaffected by ionospheric refraction, Eq. (2) making measurements at multiple receiver stations aligned with the plane of the rocket trajectory, (3) employing state-of-the-art ground receivers capable of detecting 0.001 TEC Unit (1 TECU=10^{16} m^{-2}), and Eq. (4) applying modern algorithms for the reconstruction analysis.

The next section describes the DBB experiment for measurements of TEC during the flights of the SEEK-2 rockets. This is followed by a summary of the observations at three stations located within 60 km of the rocket launch site. The data are processed to yield the electron density profiles on the upleg and downleg portions of the trajectory as the radio beacon penetrated the sporadic-E layers. More involved

analysis is used to produce the first two dimensional image of the sporadic-E layer based on computerized ionospheric tomography. The final section of the paper compares the observations with prevailing theories of sporadic-E formation and gives suggestions of improvements for future radio beacon studies of the E layer using rocket borne beacons.

2 Radio beacon experiment on SEEK-2

Rocket beacon transmissions to study the ionosphere have been described by Bernhardt et al. (1993). Briefly, two continuous wave signals at frequencies f_1 and f_2 are radiated using antennas attached to the rocket skin. The phase recorded by ground receivers is affected by both the range to the rocket (S) and the integral of the electron density ($I=\int n_e ds$) along the propagation path. The received phase in Radians is

$$\phi_i(f)=\frac{2\pi f_i}{c}S+\frac{2\pi 80.6}{2f_i c}I \quad (1)$$

where index i=1 or 2 depending on frequency. The total electron content (TEC) is obtained from the differential phase formula

$$I=\left(\phi_1-\frac{\phi_2}{N}\right)\Big/\left[\frac{2\pi 80.6}{2f_1 c}\left(1-\frac{1}{N^2}\right)\right] \quad (2)$$

where $N=f_2/f_1$ is the transmitter frequency ratio. Since TEC is determined using phase, 2π ambiguities in the phase measurement can lead to ambiguities in the TEC determination. Equation (2) is applicable if the ionospheric is smooth enough that the diffraction effects are not important. If the phase front for the radio waves passing through the ionosphere is severely distorted, diffraction of the wave may contribute to the received phase. Also, the propagation paths are assumed to be straight lines. Propagation along steep density gradients may bend the paths. In all the measurements of SEEK-2 the E-region refractive index fluctuations for the DBB signals are much less than unity and the diffraction and refraction effects can be neglected.

The Dual Band Beacon (DBB) experiment on each of the two SEEK-2 rockets used a transmitter to provide two VHF/UHF electromagnetic signals at f_1=149.988 and f_2=399.932 MHz, respectively. These unmodulated signals have a frequency ratio of 8/3. The same frequencies are also used by the Naval Ionospheric Monitoring System (NIMS) on the Oscar (TRANSIT) satellites. Slightly higher frequencies will be transmitted by the Naval Research Laboratory CERTO beacons scheduled to be launched into low-earth-orbit between 2005 and 2008 (Bernhardt et al., 2001). Four Coherent Ionospheric Doppler (CIDR) Receivers provided by the Applied Research Laboratory at the University of Texas in Austin were deployed in Japan to receive the beacon signals. These receivers use the differential phase technique to provide the Total Electron Content (TEC) from the rocket to each ground site during the period of the rocket flight.

TEC obtained by a dual frequency beacon from a sounding rocket is different from that obtained by an orbiting satellite.

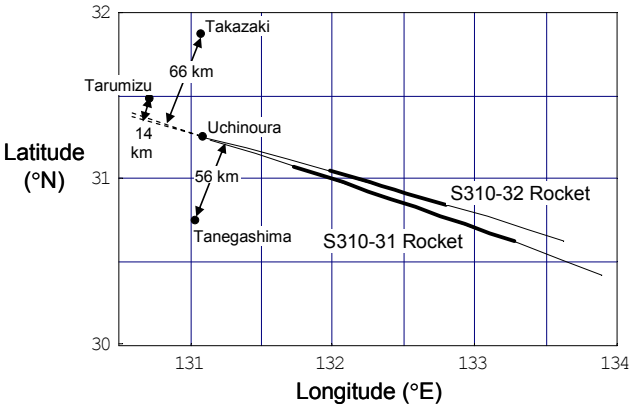

Fig. 1. Map of the trajectories of the SEEK-2 rockets relative to the four radio beacon sites on the ground.

First, the sounding rocket is launched from below the ionosphere, penetrates the ionosphere, and eventually impacts the earth. In contrast, the satellite spends its entire orbit above the bulk of the F-region plasma. Both the sounding rocket and the satellite radiate from antennas attached to the spacecraft. The rapid spin of the rocket provides rapid phase and amplitude modulations in ground receivers that usually complicates the analysis of the TEC data whereas a stabilized satellite radiates slowly varying amplitude and phase signals as it passes over a ground station. By tracking the phases of the rocket beacon signals from the ground (where the TEC is zero), through the ionosphere and down to the impact point (where the TEC is again zero), the absolute TEC can be determined without any 2π phase ambiguities. An absolute TEC measurement from satellite beacons is often prohibited by the 2π phase ambiguities. For the absolute TEC to be determined from a rocket beacon, the ground receiver must maintain continuous lock on the beacon signal. Loss of lock more than once during the flight prohibits the direct determination of absolute TEC.

The locations of the receivers and a projection of the rocket trajectories are shown by the map in Fig. 1 and the side view of Fig. 2. The two rockets were launched from Uchinoura on Kyushu, Japan. The S310-31 rocket was launched on 3 August 2002 at 23:24 JST (14:24 GMT) and S310-32 was launched precisely 15 min later. The trajectories carried the rockets into the Pacific Ocean for a non-recoverable splash down. The two sites at Takazaki and Tanegashima were located 66 and 56 km, respectively, on either side of the planes defined by the rocket trajectories. The site at Tarumizu was located to be near the plane of the trajectory so that tomographic imaging could be attempted in that plane. The dashed lines in Fig. 1 are a backward extension of the lines of the trajectories. The Tarumizu site is 14 km to the southwest of the trajectory plane for the SEEK-2 rockets.

The dark portions of the trajectories in both Figs. 1 and 2 illustrate the portion above 105 km altitude. During this portion, the radio beacon transmitting signals through the E-region. The apogees of the S310-31 and S-310-32

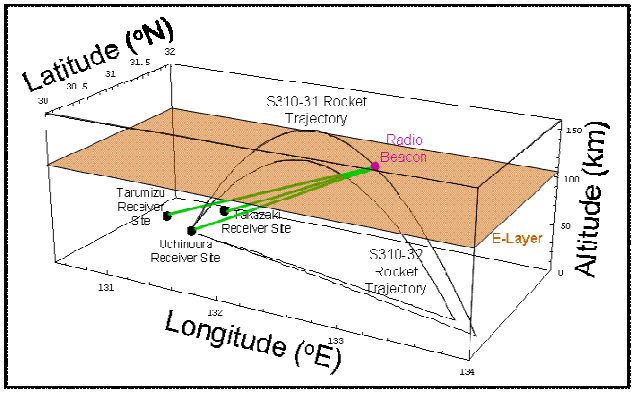

Fig. 2. Three-dimensional projection of the SEEK-2 rocket transmitting to ground receivers.

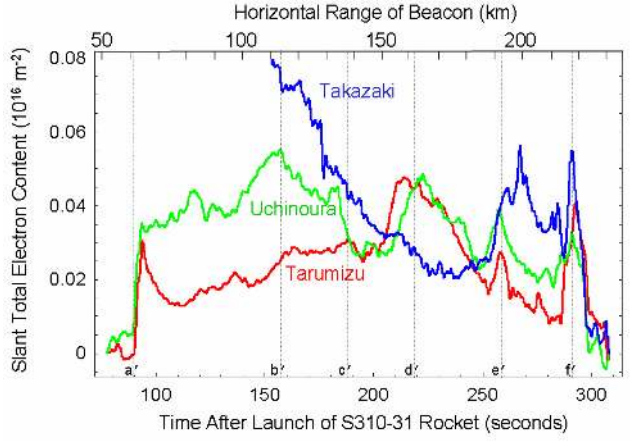

Fig. 3. TEC data from the DBB instrument on the first SEEK-2 rocket launched on 3 August 2002 at 14:24 GMT. The **(a)** Tarumizu and **(b)** Uchinoura data are recorded near the plane of the rocket trajectory. The **(c)** Takazaki data is obtained from a receiver 66 km away from this plane.

rockets were 151.88 and 116.63 km, respectively. The rockets apogee was kept low enough to keep the rocket from entering the overlying F-region. The paths to three of the receivers from a point on the trajectory show that the slant TEC in the E region is measured at multiple points at each time in the rocket flight. Both in-situ measurements and ground ionosonde records indicate that all of the plasma below 152 km altitude was confined to a 10 km region around 105 km altitude. This permits the radio beacon data to be analyzed using the thin-layer computerized tomography described later.

3 Radio beacon observations

Useful TEC data were recorded at the Uchinoura, Tarumizu, and Takazaki ground sites. Some data were obtained at Tanegashima but there were too many signal dropouts for easy interpretation. Interference from the MF radars located near the Tanegashima receiver station may have contributed to these dropouts. The resolution of the TEC data is 10^{13} m^{-3} (10^{-3} TEC Units) and the accuracy is better than 5 10^{-3} TEC Units. This accuracy is 10 to 100 times larger than usually obtained with satellite beacons. The unusually high accuracy is achieved because range to the radio beacon payload is much less than the typical range to an orbiting satellite with a TRANSIT or CERTO beacon. The received signal to noise ratio from the rocket experiment was typically 10 to 20 dB larger than for satellite observations. The increased signal to noise translates into lower noise for phase measurements in the ground receivers and higher accuracy for values of absolute TEC.

Analysis of the data at NRL required several steps before TEC could be acquired. The S310-31 and S310-32 rockets were spinning at frequencies of 0.72 and 0.90 Hz, respectively. This spin Doppler had two effects. First, the spin produced constant shifts of 0.72 or 0.90 Hz at both the VHF and UHF frequencies. This is the result of transmitting from a linearly polarized antenna on the spinning rocket to a circularly polarized antenna at each receiver site. The differential analysis scales the phase by the transmitter frequency ratio of 8/3 to determine TEC. The spin Doppler produces a linear temporal increase in TEC that must be removed. Fortunately, the rate of the TEC shift is constant and removal is accomplished by subtraction of a linear fit to the data.

The spin also introduces a modulation to the phase. This is a result of variations in the radiation pattern from the antenna around the rocket. These variations are in both amplitude and phase. The phase variations produce corresponding ripple in the TEC recovered from the data. The TEC ripple is removed using a low pass filter with a cutoff frequency of 1 Hz. The final step in the processing of the TEC data is introducing an offset so that the beginning and end values of the TEC data samples are zero.

The filtered TEC data for the flight of the first SEEK-2 rocket (S310-31) is shown in Fig. 3 as a function of time after launch. The time for the over-flight of the E layer was 200 s. Some of the same features are found in the observations for the three ground sites. Dotted lines are used to emphasize the synchronous nature of the data. At 90 s after launch (a'), the rocket enters the ionosphere and simultaneously at all sites the TEC jumps up by 0.02 to 0.03 TEC Units (10^{16} m^{-2}). The receiver at Takazaki (Fig. 3 blue) then loses lock and the early part of the data is lost. The Tarumizu site (Fig. 3 red) and the Uchinoura site (Fig. 3 green) maintain lock throughout the flight. After the initial TEC jump, the TEC at Tarumizu drops while the TEC at Uchinoura slowly increases. For a uniform layer, the TEC should slowly change according to the variations of the slant paths through the layer to the receiver. The differences between the Tarumizu and Uchinoura sites indicate the spatial differences in the E-region. The similarities result from the ray path of the beacon signals passing though similar parts of the E-region at slightly different times. The shoulder between 157 s and 188 s (b' and c'), and the peaks near 219 s (d'), 259 s (e') and 290 s (f') for Figs. 3a and b illustrate common features for receivers located near the plane of the rocket trajectory.

The Takazaki data is only available after 150 s after launch. The Takazaki site is 66 km out of the plane defined by the rocket trajectories. At this distance, there are likely to be significant differences in the TEC through the sporadic-E layer. Initially (b'), the Takazaki TEC is two to three times larger than the TEC at Uchinoura or Tarumizu. Later (d') there is a minimum Takazaki TEC whereas both Uchinoura and Tarumizu show peaks near that time in Fig. 3. Then near launch plus 270 s a peak in the Takazaki data is coincident with a drop in the TEC from the other two sites. Some common features between all three sites are found at f' just before the rocket passes through the E-layer and the three intersection points in the E-layer converge.

The second SEEK-2 rocket (310–32) was launched 15 min after the first. Because of the lower apogee of this rocket, the time for the over-flight of the E layer was only 150 s. The TEC data from Tarumizu (Fig. 4) shows significant changes in this time interval. The maximum TEC is about two times larger than obtained during the flight of the first rocket.

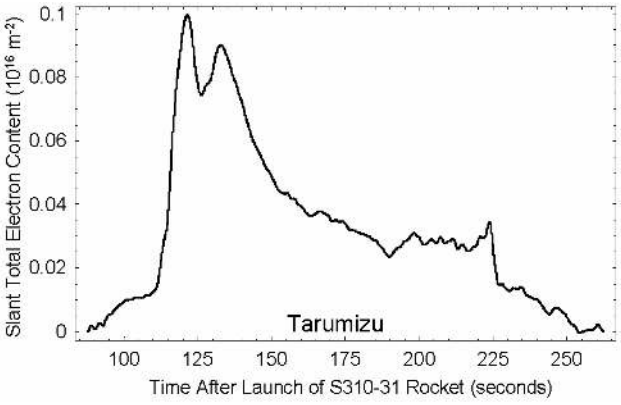

Fig. 4. TEC data from the DBB instrument on the second SEEK-2 rocket launched on 3 August 2002 at 14:39 GMT.

4 Data interpretation: layer profiles

The SEEK-2 DBB data is analyzed to provide both electron density profiles and two-dimensional images of the E layer. As the radio beacon passes through the ionosphere, the total electron content increases as the rocket penetrates deeper into the layer and more electrons are found between the radio beacon and the ground. The change in TEC for a change in rocket position has the units of electron density. Finding the electron density profile using radio beacon penetration of the layer yields a quantity called apparent electron density (Bernhardt et al., 1993). The apparent electron density will be defined to equal the absolute electron density for a layer that has no horizontal density gradients.

The first step in finding the apparent electron density is to translate the slant TEC measurements into equivalent vertical TEC. This is accomplished with the simple formula

$$VTEC(h) = \text{Slant } TEC \ \frac{h}{S} \tag{3}$$

where h is the altitude of the rocket and S is the slant range from the radio beacon to the receiver. The values for vertical TEC are computed assuming that the radio paths pierce the E-layer at 105 km altitude. Figure 5 illustrates the computed VTEC as a function of the horizontal range to the 150 km pierce altitude. This TEC mapping gives the VTEC that would be measured in an infinitely thin E layer at that altitude. If the layer had zero thickness at 105 km altitude, the curves for Uchinoura and Tarumizu near the plane of the rocket trajectory would overlap. Figure 5a shows that the data from these two sites are distinct and they only overlap where the projected VTEC is between Uchinoura and Takazaki site at horizontal ranges of 115 through 142 km from the launch location. Both Figs. 5a and b show a rapid drop in VTEC as the range is increased. This drop occurs because, as the rocket travels away from the launch point,

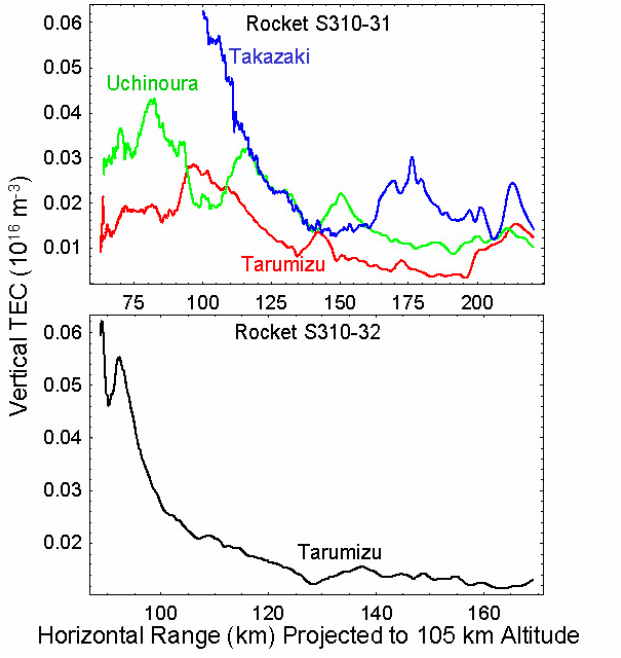

Fig. 5. Vertical TEC at 105 km altitude derived from slant TEC obtained during the flight of the **(a)** first and **(b)** second SEEK-2 rockets.

the path ΔS through the E layer becomes longer but the values of slant TEC do not increase in proportion to the path length. As the rocket moves down range, propagation paths become less vertical and the horizontal structure of the layer TEC data becomes smoothed. This loss of information degrades the tomographic reconstructions described in the next section.

The electron density at the rocket is calculated by height differentiation of the VTEC with the formula

$$N_{ea}(h) = \frac{\partial}{\partial h}\left(\frac{h}{S}\int Ne\, ds\right). \tag{4}$$

This equation gives the exact value of electron density at the rocket when Eq. (1) ray path is tangent to rocket

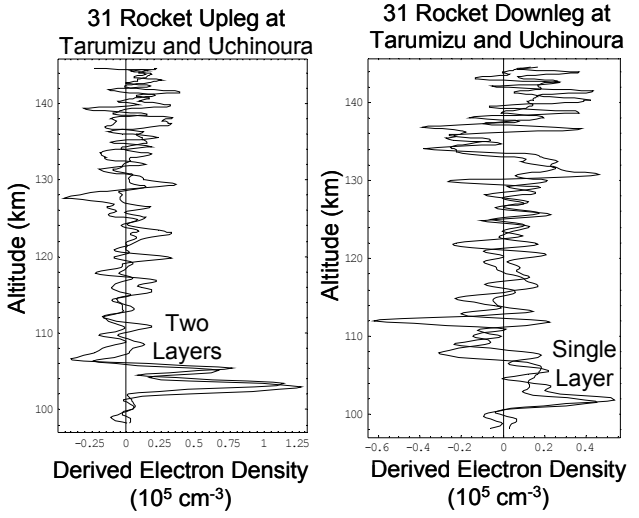

Fig. 6. Profiles of apparent electron density computed from altitude derivatives of vertical TEC. The independent measurements at Tarumizu and Uchinoura yield similar upleg and downleg profiles of electron density in the 100 to 110 km altitude range.

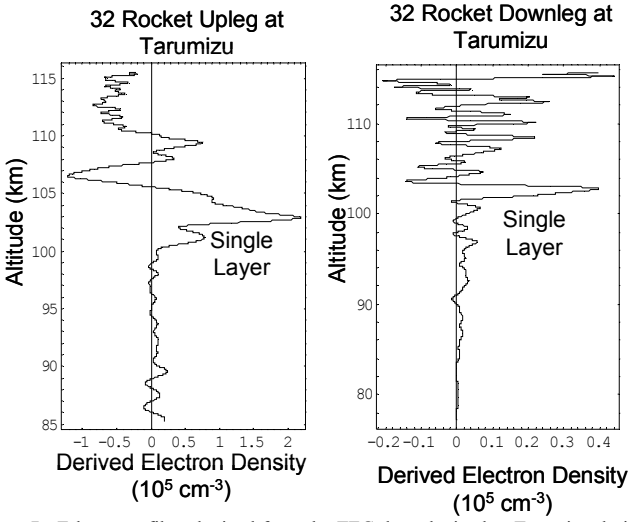

Fig. 7. E layer profiles obtained from the TEC data obtained at Tarumizu during the flight of the second SEEK-2 rocket.

trajectory or Eq. (2) the layer is horizontally stratified. Condition Eq. (1) is satisfied with the launch site (Uchinoura) data because the upleg path to the receiver is nearly along the trajectory. Because of the turbulent nature of sporadic-E, condition Eq. (2) is not expected to be satisfied.

The recovered electron density profiles from the receiver data obtained at Tarumizu and Uchinoura data are remarkably similar (Fig. 6) for both the upleg and downleg of the first SEEK-2 rocket. The upleg profiles show two layers of electron density with a peak density of about 1.2 10^5 cm^{-3} while the down leg has a single peak pf 0.5 10^5 cm^{-3} under a broad layer with a density around 0.15 10^5 cm^{-3}. The fluctuations above 100 km are obtained by differentiating the

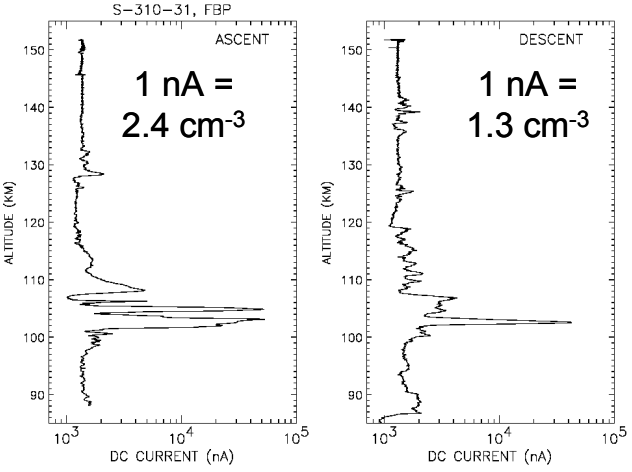

Fig. 8. Fixed bias probe measurements of electron density.

TEC when the radio beacon is above the E layer. The negative densities have no physical meaning because the rocket is above the layer during the time of their acquisition but they indicate that horizontal structure in the underlying layer causes the TEC to drop as the rocket altitude increases. The radio beacon profiling technique provides absolute values of electron density with about 0.5 km resolution.

Similar analysis was performed for the second SEEK-2 rocket (Fig. 7). Both the upleg and downleg show single layers with peak densities near 2 10^5 cm^{-3} on the upleg and 0.4 10^5 cm^{-3} on the downleg. Both rockets indicate that substantially lower densities were observed on the downleg relative to the upleg penetrations of the E layer.

Data from in-situ plasma sensors on the SEEK-2 rocket are used for comparison with the DBB results. Figure 8 illustrates the electron current profile from fixed bias probe (FBP) provided on the first SEEK-2 rocket by the Communications Research Laboratory in Japan. The electron density profiles are similar to those derived from the DBB data but the resolution a factor of 5 higher. The peak electron densities from the FBP currents can be converted into electron densities. The scale factors are indicated in Fig. 8 where 1 nA gives about 2 cm^{-3} in electron density. Other comparison of Langmuir probes with dual frequency radio beacon data has been previously reported by Maeda (1970) and Johnson et al. (1980).

Another in-situ probe on the SEEK-2 rocket was the plasma density probe (NEI) which provides the absolute densities. The ratio of the NEI peak density to the peak apparent density derived from the radio beacon (N_{ap}) is given in Table I. The ratios are near unity except that the radio beacon N_{ap} on the down leg of the second SEEK-2 rocket is a factor of two lower than the plasma probe value. This discrepancy may arise on the downleg because the propagation path is far from tangent to the trajectories and the geometry for the radio beacon profiling measurement is poor.

All of the in-situ probes and radio beacon profiles show the same shapes when the rocket is flying through the sporadic-E

layers. Since the in-situ probes have higher spatial resolution the fine structure of the sporadic-E layer is better detected with them. The radio beacon technique can detect lower densities than the probes when proper frequencies are used (Maeda, 1970). In general the probes and beacons are complementary instruments when measuring the densities at the rocket. The radio beacon, however, is unique in measuring the electron densities below the rocket between the space transmitter and ground receiver. The tomographic imaging of the sporadic-E layer below the rocket is explored in the next section.

5 Data interpretation: thin layer tomography

Computerized ionospheric tomography was first demonstrated by Austen, Franke and Liu (1988) as a method to determine electron densities in a region without having to fly through this region for direct measurements with spaceborne probes. If the paths of the radio waves transverse a region with sufficient spatial and angular scans, the data set of integrated electron densities can be processed by image reconstruction techniques to provide an accurate estimate of the electron densities. When the radio wave source comes from an orbiting satellite, a chain of receivers is set up along a line parallel to the satellite orbit. The image of the electron densities are reconstructed in the plane defined by the satellite trajectory and the line of receivers. With this geometry, the ionosphere is treated as a two-dimensional object that must be reconstructed from a finite set of "projections" formed by propagating multiple frequency radio waves through the plane of the object. The differential phase technique described in Sect. 2 is used to determine the TEC projections in the reconstruction plane. This technique, called computerized ionospheric tomography (CIT), is valid if, over the time scale of the measurements, Eq. (1) the density structures in the region are time stationary, Eq. (2) new structures are not transported into the measurement surface, and Eq. (3) refraction effects are not severe enough for the paths to deviate from straight lines. The spatial resolution of the reconstructed image will be limited to the Fresnel scale of the radio measurements. The Fresnel scale is defined as $\sqrt{\lambda D}$ where λ is the wavelength and D is the distance to the object. For the SEEK-2 measurements at 150 and 400 MHz, the slant distance to the E layer is about 120 km and the Fresnel scale for the measurements is about 500 m. The resolution used for reconstruction of the ionosphere should be limited to this dimension.

Overviews of computerized ionospheric tomography (CIT) are given by Bernhardt et al. (1998) and Kunitsyn and Tereshchenko (2003). CIT divides the solution space into a finite set of orthogonal basis functions and forms a set of linear equations that relate the electron density for each basis function to the set of TEC measurements. A common set of basis functions used to analyze the TEC is an array of pixels with a constant electron density value assigned to each pixel (Fig. 9). Receivers located at points k_1=0, 1, 2,... receive

Table 1. Comparison of plasma probe and radio beacon derived peak densities.

Ratio	Rocket 31	Rocket 32
Upleg N_{ei}/N_{ap}	0.76	0.90
Downleg N_{ei}/N_{ap}	0.91	2.0

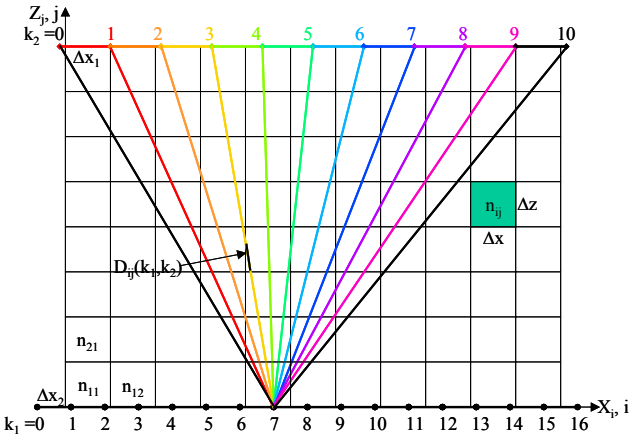

Fig. 9. Matrix of cells used to derive electron densities from a radio beacon TEC.

data from a satellite moving along a trajectory defined by points k_2=0, 1, 2,... with straight line paths between these points. The solution pixels have size Δx by Δz and the density located in the pixel at point (X_i, Z_j) is n_{ij} . Finally the distance for the path from k_2 to k_1 in pixel (i, j) is $D_{ij}(k_1, k_2)$. With this notation, the electron content along a path is represented by the linear equations

$$C(k_1,k_2)=\int\limits_{R(k_1,k_2)} N_e(x,z)dxdz=\sum_{i=1}^{N_3}\sum_{j=1}^{N_4} n_{ij}D_{ij}k_1,k_2$$

$$=\sum_{l=1}^{L(k_1,k_2)} n_{i(l,k_1,k_2)j(l,k_1,k_2)}D(l,k_1,k_2)$$

where k_1={1, ..., N_1}, k_2={1, ..., N_2}, $D(l,k_1,k_2)$

$$=D_{i(l,k_1,k_2)j(l,k_1,k_2)}(k_1,k_2), i(l,k_1,k_2),\ j(l,k_1,k_2),$$

$L(k_1,k_2)$, and $D(l,k_1,k_2)$ are fixed arrays. (5)

The TEC measurements are converted into a linear array with a path index k. Similarly, the path length is indexed by location l for path k. The details of this indexing are:

$C_k=C(k_1,k_2)$ where $k=k_1+N_1(k_2-1)$={1, ..., K}

and $K=N_1N_2$, $C_k=\sum_{l=1}^{L_k} n_{i_{lk}j_{lk}}D_{lk}$ where

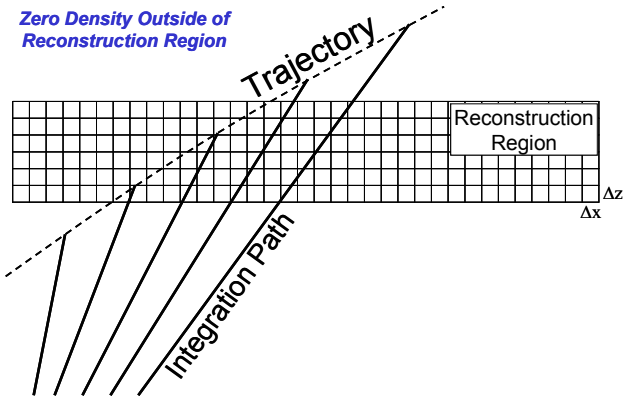

Fig. 10. Solution grid for thin layer tomography.

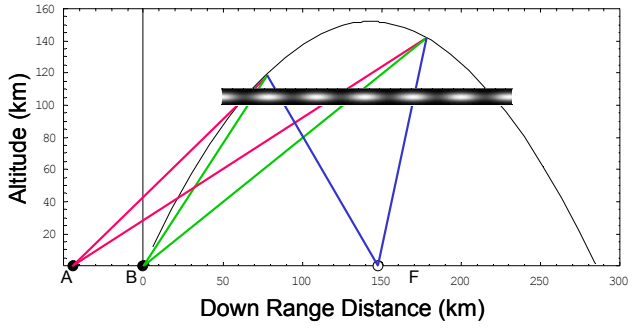

Fig. 11. Test example for tomographic reconstruction of a thin layer. The points (A, B) are the actual receiver locations at Tarumizu and Uchinoura during SEEK-2. The point F is a "fictitious" receiver located in the sea off the coast of Japan.

$$L_k{=}L(k_1,k_2),\ i_{lk}{=}i(l,k_1,k_2),\ j_{lk}{=}j(l,k_1,k_2),$$

$$D_{lk}{=}D(l,k_1,k_2),\ k_1{=}k \text{ Mod } N_1$$

$$\text{and } k_2{=}\frac{(k-k_1)}{N_1}+1.$$

Finally, the density in each pixel uses index m and the sparse matrix A_{mk} is formed as

$$C_k{=}\sum_{m=1}^{M} n_m \mathbf{A}_{mk},\ \text{where } m{=}i{+}N_3(j{-}1) \text{ ranges from 1 to}$$

$$M,\ \text{and } M{=}N_3N_4 i{=}m \text{ Mod } N_3,\ j{=}\frac{(m-i)}{N_3}{+}1,\ \text{and}$$

$$\mathbf{A}_{\mathrm{mk}} = \begin{cases} D_{lk} & \text{if } m = i_{lk} + N_3(j_{lk}-1) \\ 0 & \text{Otherwise} \end{cases} \qquad (6)$$

The linear equations in Eq. (6) have M unknowns for K measurements. One approach for the solution is the algebraic reconstruction technique (ART) which uses an iterative solution to algebraic equations. During the iteration each electron density pixel is corrected to match TEC observations. The updated pixel values get additive corrections for ART, multiplicative corrections for MART and simultaneous updates for Simultaneous Iterative Reconstruction Technique (SIRT). Details of setting up these algebraic methods are given by Bernhardt et al. (1998).

The choice of solution technique can be based on the noise in the data. The maximum a posteriori probability (MAP) is used for noisy data with a known noise covariance (Kamalabadi et al., 1999). This technique requires a statistical model for electron density and has been previously applied to space-based extreme ultraviolet (EUV) tomography of the ionosphere. The EUV measurements typically are much noisier than TEC for radio beacons because the EUV signals are very weak. When the data have low noise, the singular value decomposition (SVD) technique is recommended. This technique yields a least squares estimate of the electron density (Bernhardt et al., 1998). It has the advantage over ART by providing zero densities in regions where there is no measurement information. SVD is used in the analysis of the SEEK-2 data.

The SVD solution employs the matrix notation $C_k{=}\sum_{m=1}^{M} n_m \mathbf{A}_{mk}$ or $\mathbf{C}{=}\mathbf{A}{\cdot}\mathbf{n}$ where $\mathbf{A}$ is an (M,K) matrix. The data is modeled as having additive noise of the form $\mathbf{C}{=}\mathbf{A}\cdot\mathbf{n}{+}\mathbf{w}$. The singular value decomposition of the $\mathbf{A}$ matrix is

$$\mathbf{A}{=}\mathbf{U}\cdot\Sigma\cdot\mathbf{V}^T,\mathbf{U}\cdot\mathbf{U}^T{=}\mathbf{I},\mathbf{V}\cdot\mathbf{V}^T{=}\mathbf{I} \text{ where}$$
$$U \text{ is } (M,M),\ V \text{ is } (K,K),\ \Sigma \text{ is } (M,K) \text{ diagonal matrix}$$
$$\Sigma{=}\begin{bmatrix}\mathbf{D}\ 0\\ 0\ 0\end{bmatrix},\ \mathbf{D}{=}\begin{bmatrix}\sigma_1 & 0 & 0\\ 0 & \ddots & 0\\ 0 & 0 & \sigma_r\end{bmatrix},\ \mathbf{U}{=}\begin{bmatrix}\mathbf{u_1}\cdots\mathbf{u}_M\end{bmatrix}, \qquad (7)$$
$$\mathbf{V}{=}\begin{bmatrix}\mathbf{v_1}\cdots\mathbf{v_K}\end{bmatrix}$$

The solution with this decomposition is

$$\hat{\mathbf{n}}{=}\mathbf{V}\cdot\Sigma^I\cdot\mathbf{U}^{\mathbf{T}}\cdot\mathbf{C}{=}\sum_{k=1}^{r}\frac{\mathbf{v}_k(\mathbf{u}_k^T\cdot\mathbf{C})}{\sigma_k}{=}\mathbf{n}+\sum_{k=1}^{r}\frac{\mathbf{v}_k(\mathbf{u}_k^T\cdot\mathbf{w})}{\sigma_k} \qquad (8)$$
$$\text{where the pseudo inverse is } \Sigma^I{=}\begin{bmatrix}\mathbf{D}^{-1}\ 0\\ 0\ 0\end{bmatrix}.$$

If the noise vector $\mathbf{w}$ is zero, then the electron densities are recovered. If the noise statistics for the TEC measurements are known, then the noise in the recovered density measurements can be determined from the second term in Eq. (8). The computational formulations for Eq. (7) and Eq. (8) were implemented using Mathematica Version 5.

Along with measurement noise, the geometry of the observations limits the accuracy of the recovered electron densities. For the analysis of the SEEK-2 DBB data, a thin layer geometry is used. This geometry limits the reconstruction to a region between 100 and 110 km altitudes (Fig. 10). Restricting the solution space to this altitude range is justified by the measurements from the in-situ probes which showed that the electron densities were less than $5\ 10^3\ \mathrm{cm}^{-3}$ between 110 km and the apogees of either rocket. With tomographic solutions for the grid in Fig. 10, the electron densities are derived using data acquired both as the S310–31 rocket penetrated the layer and as the rocket flew above the E-region.

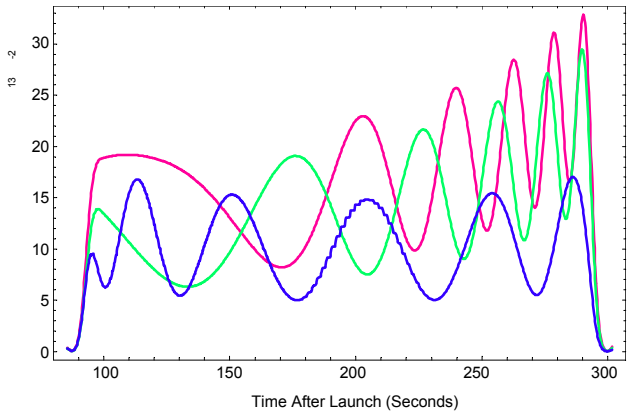

Fig. 12. Synthetic TEC for receivers located at ends of the (A) red, (B) green, and (C) blue paths in Fig. 11. The corresponding observational data with the same geometry is given in Fig. 3a for the (A) Tarumizu and (B) Uchinoura stations.

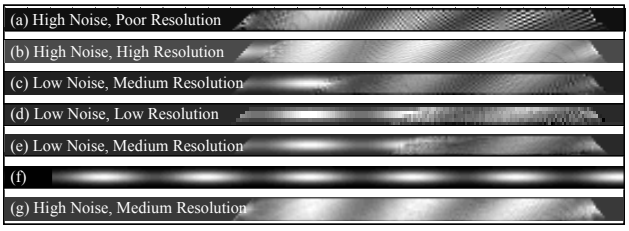

Fig. 13. SVD and MAP reconstructions of the test example with various numbers of TEC data samples and changes in the sizes of the reconstruction cells. The original model layer (f) is given for reference. The samples per receiver vary from **(a)** 106 to (**(b)** through **(d)**) 541 to (**(e)** and **(g)**) 1082. The horizontal grid cell size is fixed at 1 km. The vertical grid size varies from (b) 1/2 km to (a, **(c)**, e, and g) 1 km to (d) 2 km. The reconstruction techniques are (a through e) SVD and (g) MAP. The best reconstruction (e) matches the original **(f)** on the left half of the reconstruction region.

The profiling technique of the previous section only used data from the rockets penetrating the thin layers.

Before applying the reconstruction algorithm to the measured TEC data, a test case was formed using an analytic model for the quasi-periodic structure (Fig. 11). The structure used a Gaussian profile with a width of 2 km and a peak density of 2×10^5 cm^{-3}. This structure was modulated with a unit amplitude sinusoid and a period of 45 km. Synthetic TEC data was generated by integrating along straight line paths to three receivers along the ground from the trajectory of the first SEEK-2 rocket. Two of the receivers were located at (A) Tarumizu and (B) Uchinoura. The third receiver was placed underneath the trajectory at a range of 150 km. A third receiver at this location did not exist in the experiment but it was added to provide an indication of its value for future experiments.

The TEC data computed for the E layer model is shown in Fig. 12. This data set is used with the same algorithm that processes the measured SEEK-2 DBB data. The red and green curves in Fig. 12 can be compared to the red and green curves in Fig. 3a with the actual measurements. The slant TEC in Fig. 12 increases with time as the radio beacon paths become more oblique. In contrast, the slant TEC in Fig. 3a decreases with time indicating a substantial reduction of E-region TEC down range from the launch point. The blue curve in Fig. 12 represents the "fictitious" TEC obtained from a receiver point located at point (C) in Fig. 11.

The initial tests of the thin layer tomography algorithm only use the two sets of synthetic data from the receivers at points A and B. To optimize the reconstructions, several data sampling periods and several grid cell sizes were used. The number of samples per receiver was selected as 106, 541, or 1081. This corresponds to data sample rates of 0.5, 2.5, 5 samples per second. The lower rate samples were chosen from the simulations without any averaging of the high rate data. The horizontal grid spacing was fixed at 1 km. The vertical grid spacing was varied with 1/2, 1 or 2 km. Finally both SVD and MAP techniques were used for the algorithm tests. Fig. 13 shows the results of the reconstructions with the algorithms. The MAP produced poor results. The SVD yielded excellent results for part of the reconstruction region. Using 106 samples gave high noise and poor resolution. Increasing the samples per receiver reduced the noise in the reconstructions. As expected, increasing the vertical grid size reduced the vertical resolution. Finally, reducing the vertical grid sized to 1/2 km yielded high noise along with the high resolution. The optimum number of receiver samples and grid size, illustrated by the results just above the original in Fig. 13, were obtained with 1082 data samples using 1 km$\times$1 km square pixels.

Even with the optimum parameters, the electron density reconstructions were only adequate for the left half of the data set. Figure 14 illustrates the best reconstruction of the test data set relative to the measurement geometry. The noisy region is the result of truly independent sampling of the downrange TEC with the two receivers to the left of the launch point (B). Because of nearly parallel propagation paths for horizontal ranges past 150 km, the reconstruction was repeated with the additional data from a receiver (C) located at the 150 km range point. The addition of the third receiver data greatly improves the reconstruction over the whole layer underneath the trajectory (Fig. 15) because greater angles are obtained for the beacon to receiver paths. Future electron density imaging experiments would benefit from having at least one receiver located directly underneath the apogee of the rocket.

Additional test cases were used to validate the thin-layer tomography algorithm. Since the E-region is likely to have multiple layer structure, a two layer model was constructed with modulated layers at 102 and 105 km. The horizontal modulations have 13 and 22 km for the layer at 102 km and 30 km for the layer at 105 km altitude. The results of the tests are illustrated in Fig. 16. Along with grey-scale maps of the reconstructions, the RMS error in the attitude bins at each horizontal range is shown. The thin-layer-tomography works

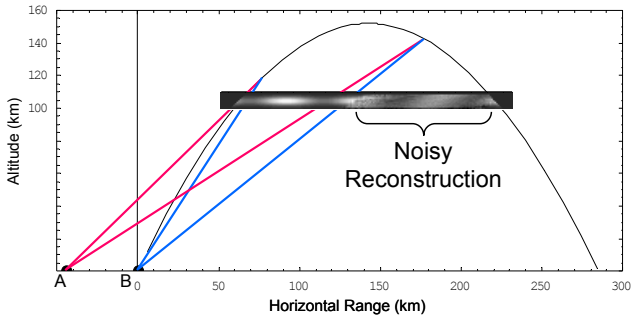

Fig. 14. SVD reconstruction of the test example using two receivers, 1082 samples per receiver (corresponding to 0.2 s time samples or 158 meter horizontal range samples) and a reconstruction grid with a 1 km (H)×1 km (V) cell size.

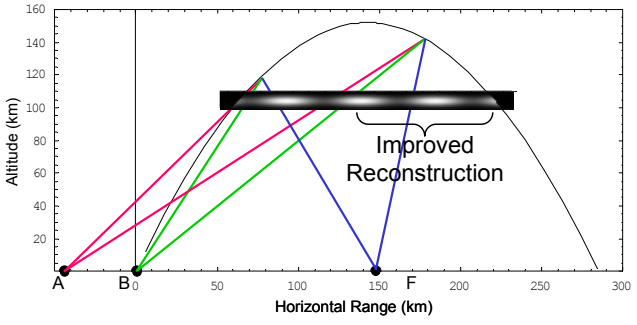

Fig. 15. SVD reconstruction of the test example using data from three receivers, 1082 samples per receiver and a reconstruction grid with 1 km (H)×1 km (V) cell size. The addition of the data from the third receiver yields the improved reconstruction region.

extremely well for multiple layers with three receivers. In all tests, the two receiver case provides a good reconstruction only on the left side. The results of this simulation clearly demonstrate that the technique can differentiate between horizontal layers a few kilometers apart.

The test case studies have shown that the SVD algorithm yields excellent reconstructions of the E layer densities beneath the rocket trajectory. The reconstructed densities faithfully replicate both magnitude and locations of the density structures. The root mean square error for the SVD technique can be very low if the noise in the measurements is low. For all the simulations of the test examples, no noise was added to the data. In practice, the noise in the TEC data is estimated to be about 0.005 TECU for 0.2 s data samples.

The two sets of TEC data (red and green lines in Fig. 3) for the first SEEK-2 rocket were processed by the thin layer SVD algorithm. The results, shown in Fig. 16, replicate many features from the test cases. As with Fig. 14, the reconstruction on the left side of the layer is relatively smooth and coherent, while the one on the right side is noisy. The detail of the reconstruction shows a thin layer at 102 km altitude centered at a range of 85 km with a horizontal width of about 30 km. There is a weak layer near 104 km centered at 88 km horizontal range with a width of 7 km. Another weaker layer is found

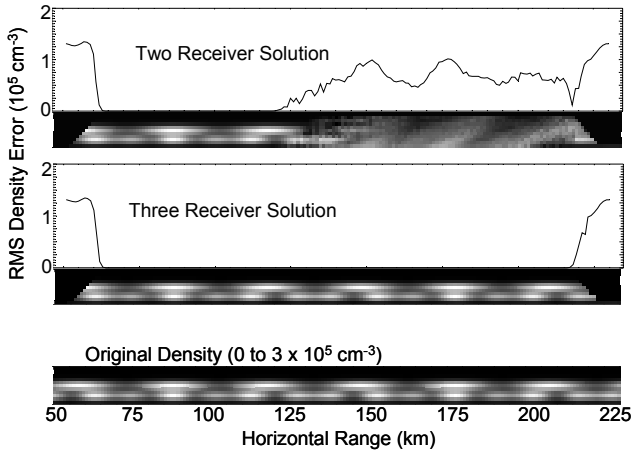

Fig. 16. Reconstructions of a multiple-layer test model of the E-layer using simulated measurements with the SEEK-2 rocket beacon transmitting to 2 or 3 ground receivers shown in Fig. 15.

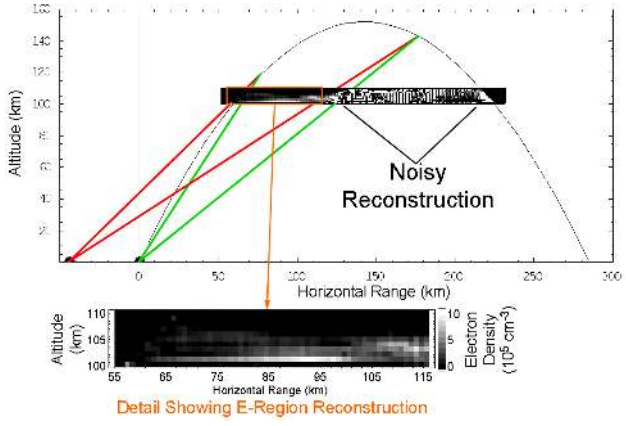

Fig. 17. SVD reconstruction of the DBB data during the flight of the SEEK-2-31 rocket using two ground Receivers, 1082 Samples Per Receiver (0.2 s time samples or 158 m horizontal range samples) and a reconstruction grid with 1 km (H)×1 km (V) cell size.

at 105 km centered near 77 km horizontal range. A slanted gap in the electron density is found near a range of 105 km. Finally, the beginnings of a dense layer with 7×10^5 cm^{-3} at 104 km are seen for ranges between 105 and 115 km. The reconstructed layer has some negative densities at the top of the reconstruction. This error in density is probably a result of the 14 km misalignment of the Tarumizu receiver station relative to the plane of the rocket trajectory (see Fig. 1). To compensate for the negative values of TEC at the top of the reconstruction, the densities are probably too large for the thin layer at the bottom. A linear correction for the negative densities yields a maximum layer density of 5×10^5 cm^{-3}.

The tomographic reconstruction gives the same densities as is provided by the apparent densities obtained on the upleg of the rocket as it passes through the ionosphere. This is not surprising since the thin layer tomography uses the same TEC data was is used for the apparent density calculation

illustrated by Fig. 6. We have not added the in situ data to the reconstruction because we do not feel that the added high resolution would improve the density determination on the 1 km scale of the reconstructions.

6 Summary and conclusions

The analysis of the SEEK-2 radio beacon data showed wide variations in sporadic-E layer structures between ground receiver sites and flight trajectories of the two rockets. Horizontal E layer variations were recorded with 10 to 50 km scale sizes. Vertical profiles of electron densities showed both double and single layers. Calibration and validation of DBB based density measurements were obtained by examining the electron densities from the in-situ probes on the SEEK-2 rockets. The first tomographic image of a sporadic-E layer was produced using a thin layer tomography solution. The "in-plane" TEC data from the Uchinoura and Tarumizu receiver sites during the flight of the first SEEK-2 rocket was used for the analysis. The reconstructed densities show multiple thin layers of limited horizontal extent.

The radio beacon technique for E layer imaging should be used for future rocket experiments. The technique has been validated for E-region studies using both synthetic and actual TEC data. More ground receivers would improve the accuracy of the reconstructed image. A receiver directly under the apogee of the trajectory is essential for complete imaging of the E layer in the measurement region. The receivers should be aligned within 1 km of the plane of the rocket trajectory. Several of the receivers suffered from "loss of lock" of the beacon signals. This may be the result of radio interference, nulls in the antenna pattern from the payload, or scintillations from the E-region irregularities. Interference from the radar sites at Tanegashima were thought to have disabled one of the ground DBB receivers. For future experiments, the pattern of the antennas on the rocket should be carefully checked for nulls. The signal dropouts may have been the result of the irregularity structures in the E layers. Maruyama (1995) has reported greater than 10 dB signal reductions of VHF radio signals from satellite beacons passing over sporadic-E layers. The receivers used in the experiment only recorded TEC and not amplitude. Future experiments also should add the capability of amplitude measurements so that scintillation data could be obtained. Amplitude diffraction patterns could validate the theory of Maruyama et al. (2000) that field aligned irregularities with tens of km lengths could be responsible for quasi-periodic radar echoes.

With proper experimental geometry, the relationship between electron density fluctuations and electric fields in sporadic-E layers can be observed. Polarization electric fields that couple the E- and F-regions affect the evolution of the density irregularities (Bernhardt 2002; Yokoyama et al., 2004). Large scale electric fields produce the drifts of the density irregularities. Closely spaced receivers could provide drift measurements by correlating the amplitude fluctuations during the rocket flight. If the rocket experiments are launched along the magnetic meridian, E-field probes could detect the electric fields that map along magnetic fields from electron density structures determined using computerized ionospheric tomography using rocket borne radio beacons. This comparison was not attempted during the SEEK-2 experiments because the rocket trajectories flew nearly perpendicular to the magnetic meridians.

Acknowledgements. This work was supported at NRL by grants from Institute of Space and Aeronautical Science (ISAS) and the Office of Naval Research (ONR). The authors are grateful for encouragement and support of H. Hayakawa and the ISAS rocket team. F. Kamalabadi of UIUC suggested the use of the SVD reconstruction algorithm and Y. Kamata and K. Kawahara of ISAS provided the 150 MHz antenna on the rocket.

Topical Editor M. Pinnock thanks S. Franke and J. A. Secan for their help in evaluating this paper.

References

Austen, J. R., Franke, S. J., and Liu, C. H.: Ionospheric imaging using computerized-tomography, Radio Sci. 23, 299–307, 1988.

Bernhardt, P. A., Huba ,J. D., Charturvedi, P. K., Fulford, J. A., Forsyth, P. A., Anderson, D. N., and Zalesak, S. T.: Analysis of Rocket Beacon Transmissions to Reconstruct Ionospheric Densities, Radio Sci., 28, 613–627, 1993.

Bernhardt, P. A and Huba, J. D.: Reconstruction of non-stationary plasma irregularities using ionospheric tomography, Cospar Colloquia Series: Low-Latitude Ionospheric Physics, Taipei, November, 1993.

Bernhardt, P. A., McCoy, R. P., Dymond, K. F., Picone, J. M., Meier, R. R., Kamalabadi, F., Cotton, D. M., Chakrabarti, S., Cook, T. A., Vickers, J. S., Stephan, A. W., Kersely, L., Pryse, S. E., Walker, I. K., Mitchell, C. N., Straus, P. R., Na, H., Biswas, C., Bust, G. S., Kronschnabl, G. R., and Raymund, T. D.: Two-dimensional mapping of the plasma density in the upper atmosphere with computerized ionospheric tomography (CIT), Phys. Plas., 5, 2010–2021, 1998.

Bernhardt, P. A., Huba, J. D., Selcher, C. A., Dymond, K. F., Carruthers, C. R., Bust, G., Rocken, C., and Beach, T. L.: New Systems for Space Based Monitoring of Ionospheric Irregularities and Radio Wave Scintillations, Space Weather, Geophysical Monograph 125, 431–440, AGU, 2001.

Bernhardt, P. A.: The modulation of sporadic-E layers by Kelvin-Helmholtz billows in the neutral atmosphere, J. Atm. Solar-Terr. Phys., 64 , 1487–1504, 2002.

Bernhardt, P. A., Gondarenko, N. A., Guzdar, P. N., Djuth, F. T., Tepley, C. A., Sulzer, M. P., Ossakow, S. L., and Newman, D. L.: Using Radio Induced Aurora to Measure the Horizontal Structure of Ion Layers in the Mesosphere and Lower Thermosphere, J. Geophys. Res., (108), 1336–1346, 2003.

Cosgrove, R. B. and Tsunoda, R. T.: Instability of the E-F coupled nighttime midlatitude ionosphere, J. Geophys. Res., 109(A04305), 2004.

Djuth, F. T., Bernhardt, P. A., Tepley, C. A., Gardner, J. A., Kelley, M. C., Broadfoot, A. L., Kagen, L. M., Sulzer, M. P., Elder, J. H., Isham, B., Brown, C., and Carlson, H. C.: Production of large airglow enhancements via wave-plasma interactions in sporadic-E, Geophys. Res. Lett., 26, 1557–1560, 1999

Evans, J. V.: Satellite beacon contributions to studies of structure of the ionosphere, Rev. Geophys., 15, 325–350, 1977.

Friedman, H.: Rocket observations of the ionosphere, Proc. Inst. Radio Eng., 46, 272–280, 1959.

Fulford, J. A., MacDougall, J. W., Forsyth, P. A., Mendillo, M., and Bernhardt, P. A.: Ionospheric electron content measurements during the second space-plasma negative-ion experiment (SPINEX-2), Canadian J. Phys., 65, 403, 1987.

Haldoupis, C., Bourdillon, A., Kamburelis, A., Hussey, G. C., and Koehler, J. A.: 50 MHz continuous wave interferometer observations of the unstable mid-latitude E-region ionosphere, Ann. Geophys., 21, 1589–1600, 2003.

Jackson, J. E.: Measurements in the E layer with the Navy Viking rocket, J. Geophys. Res., 59, 377–390, 1954.

Johnson, C. Y., Sjolander, G. W., Oran, E. S., Young, T. R., Bernhardt, P. A., and da Rosa, A. V.: "F Region over Kauai: Measurement, Modeling, and Modification," J. Geophys. Res., 85, 4205, 1980.

Kagan, L. M., Kelley, M. C., Garcia, F., Bernhardt, P. A., Djuth, F. T., Sulzer, M. P., and Tepley, C. A.: The structure of electromagnetic wave-induced 557.7-nm emission associated with a sporadic-E event over Arecibo, Physical Review Letters, 85, 218–221, 2000.

Kamalabadi, F., Karl, C. W., Semeter, J. L., Cotton, D. M., Cook, T. A., and Chakrabarti, S.: A statistical framework for space-based EVUV ionospheric tomography, Radio Sci., 437–447, 1999.

Kunitsyn, V. E. and Tereshchenko, E. D.: Ionospheric Tomography, Springer, 2003.

Larsen, M. F.: A shear instability seeding mechanism for quasiperiodic radar echoes, J. Geophys. Res., 105, 24 931–24 940, 2000.

Layzer, D.: The turbulence criteria in stably stratified shear flow and the origin of sporadic E, in: Ionospheric sporadic-E (Eds.) Smith, E. K. and Matsushita, S., 258–275, Macmillan, 1962.

Leitinger, R., Jakowski, N., and Davies, K., et al.: Ionospheric electron content and space weather: Some examples, Phys. Chem. Earth, Part A-Solid Earth and Geodesy, 25, 629–634, 2000.

Maeda, K. I.: Radio propagation effects used on rockets in probing the ionosphere, J. Atm. Solar-Terr. Phys., 32, 647, 1970.

Maruyama, T.: Shapes of irregularities in the sporadic-E layer producing quasi-periodic scintillations, Radio Sci., 30, 581–590, 1995.

Maruyama T, Fukao, S., and Yamamoto, M.: A possible mechanism for echo striation generation of radar backscatter from midlatitude sporadic E, Radio Sci., 35, 1155–1164, 2000.

Miller, K. L. and Smith, L. G.: Incoherent-scatter radar observations of irregular structure in the mid-latitude sporadic-E layers, J. Geophys. Res., 83, 3761–3775 1978.

Smith, E. K. and Matsushita, S.: Ionospheric sporadic-E, Macmillan, 1962.

Smith, L. G. and Gilchrest, B. E.: Rocket Observations of electron-density in the nighttime E-region using Faraday-rotation, Radio Sci., 19, 913–924, 1984.

Whitehead, J. D.: Production and prediction of sporadic-E, Rev. Geophys. Space Phys., 8, 65, 1970.

Woodman, R. F., Yamamoto, M., and Fukao, S.: Gravity-wave modulation of sporadic-E irregularities, Geophys. Res. Lett., 18, 1197–1200, 1991.

Yamamoto, M., Fukao, S., Woodman, R. F., Oga, W. T., Tsuda, T., and Kato, S.: Midlatitude E-region field-aligned irregularities observed with the MU radar, J. Geophys. Res., 96, 15 943–15 949, 1991.

Yamamoto, M., Komoda, N., Fukao, S., Tsunoda, R. T., Oga, W. T., and Tsuda, T.: Spatial structure of the E-region field-aligned irregularities revealed by the Mu radar, Radio Sci., 29, 337–347, 1994.

Yamamoto, M., Ono, T., Oya, H., Tsunoda, R. T., Larsen, M. F., Fukao, S., and Yamamoto, M.: Structures in sporadic-E observed with an impedance probe during the SEEK campaign: Comparisons with neutral-wind and radar-echo observations, Geophys. Res. Lett., 25, 1781–1784, 1998.

Yokoyama, T., Yamamoto, M., and Fukao, S., et al.: Three-dimensional simulation on generation of polarization electric field in the midlatitude E-region ionosphere, J. Geophys. Res., 109(A01309), 2004.